Rotor wake engineering models for aeroelastic applications

IOP Conf. Series: Journal of Physics: Conf. Series **1037** (2018) 062013 doi:10.1088/1742-6596/1037/6/062013

Rotor wake engineering models for aeroelastic applications

Koen Boorsma[1], Luca Greco[2], Gabriele Bedon[1]

[1]ECN part of TNO, Westerduinweg 3, 1755 LE Petten, The Netherlands
[2]CNR-INSEAN, Marine Technology Research Institute, Via di Vallerano 139, Rome, Italy

E-mail: koen.boorsma@tno.nl

Abstract. Results from the EU AVATAR project have indicated vortex methods generally to be in good agreement with computational fluid dynamics simulations for resolving rotor aerodynamic forces in a variety of operational and inflow conditions. Limitations of the more crude blade element momentum method, most widely used in industry, have been exposed. Although not as expensive as computational fluid dynamics, the application of vortex methods to resolve rotor aerodynamics in wind turbine design and loads calculations is still hindered by its computational burden. An increase in computer power and parallelization has helped over the decades, but an efficiency boost is required to make the last step. The effect of simplifying the far wake description on predicted loads as well as computational effort is investigated for a variety of load cases. Results indicate that dynamic and time averaged loading characteristics are preserved when the mid to far wake grid resolution is reduced. The applied wake reduction is a promising technique leading to desktop design load calculations using vortex wake methods.

1. Introduction

The design of larger turbines with lighter and more flexible blades relies on the integration between accurate unsteady aerodynamics, structural dynamics and control within fast comprehensive numerical tools. Within the EU AVATAR project [1], the accuracy of large rotor aerodynamic simulations has been investigated by comparing different fidelity models and experiments for a variety of operational and inflow conditions [2]. State-of-the-art aerodynamics codes used for design load calculations are currently based on well-assessed engineering blade element momentum (BEM) models. Computational fluid dynamics (CFD) tools are increasingly showing their capability to achieve a physically consistent description of turbine flow-field, but they are still not well suited for aeroelastic analyses in practical preliminary design and certification. In this scenario, potential-flow methods represent an advanced convenient solution to overcome the limitations of BEM codes to fill the gap with complex and time consuming CFD simulations. Still, the wide use of these models for wind turbine aeroelastic design load calculations requiring simulation time steps in the order of 1° rotor azimuth or smaller, has been hindered by the computational effort necessary for an accurate description of blade wake dynamics. Thus, although parallelization goes a long way in reducing the burden, an efficiency step has to be made. Several efforts to overcome this bottleneck have been undertaken in the past. Prescribing wake geometry [3] rather than engaging in the costly nonlinear procedure based on Biot-Savart law to align the wake with the local flowfield [4] fails to bring accuracy in transient and dynamic load case calculations. More recently, a fast multilevel integral transform [5] has

been applied to a panel method to reduce CPU-time for the simulation of turbine rotor wake flow. Alternatively, effective *hybrid wake* techniques simplifying the far wake description in comparison to the near wake have been proposed [6–9]. Within these methodologies, the present paper investigates a cost-effective free-wake model that requires limited programming effort to the existing codes and can be considered as an engineering method making approximations to vortex wake theory.

2. Rotor wake engineering models

Vortex wake methods for the solution of the potential flow around turbine blades rely on the discretization of the wake into a network of shed and trailing vortices and on free-wake algorithms to align the rotor wake to the local induced flowfield. This nonlinear iterative process, acknowledging the fact that a suitable wake length behind the turbine has to be taken into account, has a severe impact on the memory and CPU-time requirements of the simulation. A significant reduction of computational costs is herein achieved by splitting the wake into a near, a transition and a far portion. A free-wake approach presenting a full lattice dimensioned by spanwise and temporal resolution is used within the near wake. Differently, the transition wake is simplified by progressively neglecting the effect of shed vortices, preferably only retaining the influence of trailing vortices at the far wake end. Two different methods to make the wake treatment more efficient are attempted as described below.

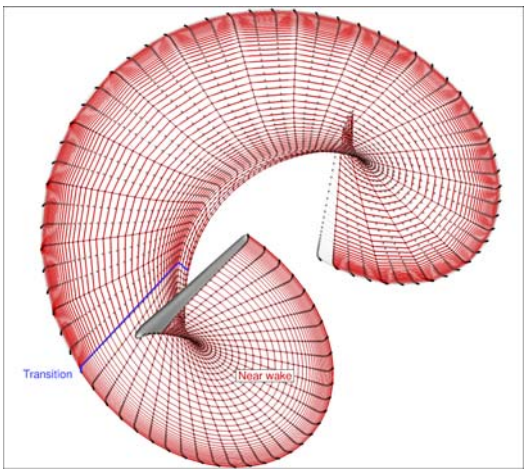

(a) Grid coarsening after half a revolution (red lines) compared to fine wake grid (black lines).

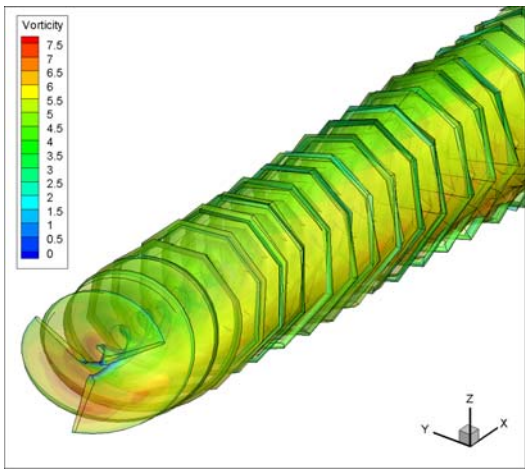

(b) Wake shape prediction (3 shed vortices are skipped after one revolution).

Figure 1. Illustration of the applied rotor *wake reduction* technique.

2.1. Wake reduction

The CPU-time saving is achieved by decreasing the total number of wake points through coarsening grid resolution in streamwise direction after the near wake region. An example of this technique is shown in Figure 1(a), where, for clarity, the transition zone is started after half a rotor revolution, skipping two streamwise wake points as depicted in red (the fine wake grid being in black). During blade revolution, at each time step a new sheet is shed into the wake. The *wake reduction* technique allows to uncouple the time discretization of the problem from the streamwise spatial resolution of the wake. Indeed, after the transition line (in blue in Figure 1(a)) the effective time step for wake sheets convection is increased (triple in this example) whilst the time discretization for the numerical solution of the problem remains unchanged. Hence, due

to the reduction, in this example two shed vorticity lines are discarded and the trailing vorticity is distributed along a straight path spanning a larger azimuth step. In this way, the vorticity shedding process from one lattice element to the next one in streamwise direction is applied to wake elements of increasing azimuthal dimension. In practical applications, the transition zone is further downstream (*e.g.* after one rotation, like illustrated in Figure 1(b)). Also, a more ideal approach would include multiple transition zones, and not only skipping shed vorticity lines but also mid-span trailing vorticity. Alternatively an analytical formulation representing a cylindrical wake may be used to account for the far wake from a certain downstream distance.

2.2. Shed skipping

One of the bottlenecks of free-wake algorithms is the evaluation of the induced velocity on wake and blade points through the Biot-Savart law. The *shed skipping* technique aims to reduce the CPU-time demand of this computation whilst keeping a streamwise constant surface discretization along the wake. Hence, this approach skips wake points only during evaluation of the Biot-Savart law rather than really removing them from the wake grid. To this aim, all the shed vortices in the near wake are retained; then, in the transition wake, a skip function is applied to gradually neglect shed contributions. Differently, in the far wake, all shed vortices are neglected whilst trailing vortices are all retained up to a prescribed distance from rotor plane. Finally, only tip and root vortices are taken into account.

3. Implementation and validation strategy

The proposed wake models are implemented into a generalized lifting line theory and a 3D unsteady panel method and applied for a number of load cases to assess their accuracy and CPU-time saving. A brief overview of the used solvers is provided further in this section. For both techniques the streamwise position of the start(s) of the coarsening and the degree of coarsening itself are varied, which can be compared to a reference without coarsening. To enable a proper comparison, the full wake length in terms of convected distance was kept the same between reference and coarsened simulations. BEM results are calculated as well allowing to identify the added value of the vortex wake methods. To give the comparison a physical reference, measured load cases from the New Mexico wind tunnel campaign [10] have been used where possible. This test features the fully instrumented 4.5 m diameter three bladed Mexico rotor with variable speed and pitch control, tested in the large open jet facility of the German Dutch Windtunnels DNW. A comparison is made using the sectional loads obtained from the fast pressure sensors instrumented at five different spanwise sections (25%, 35%, 60%, 82% and 92%R). Since the measured values at the 60%R station were suspect (outlier), these were replaced using linearly interpolated values from the nearest stations. Chord normal and tangential sectional forces are obtained by integrating the measured pressure distributions along the local chord. Rotor integral variables such as axial force and torque are obtained by integrating these along the span. To prevent differences due to the limited number of sensors, the experimental resolution in spanwise direction is used to obtain these from the simulations. An experimental uncertainty is estimated assuming an uncertainty in the pressure sensors of 35 Pa. The solid aluminium blades are considered rigid, hence the simulations featuring the Mexico rotor do not include aeroelastic interaction.

3.1. Aerodynamics codes

Both a generalized lifting line theory and a 3D unsteady panel method for the analysis of inviscid flows around lifting bodies in arbitrary motion are considered to address turbine rotor aerodynamics modelling. The used codes and the featured settings are described below.

The **ECN Aero Module** [9, 11] features a BEM method similar to the implementation in Phatas [12] and a free vortex wake code in the form of AWSM [13]. AWSM models the wake geometry by convecting shed and trailing vorticity into a vortex lattice. Here the trailing vorticity accounts for the effects of spanwise circulation variation, whilst the shed vorticity accounts for the effects of bound vortex variation with time. Both models are lifting line codes and they make use of aerodynamic look-up tables to evaluate airfoil performance. Several dynamic stall models, 3D correction models, wind modeling options and a module for calculating tower effects are included. The set-up allows to easily switch between the two aerodynamic models whilst keeping the external input the same, which is a prerequisite for a good comparison between them. The package is coupled to the FOCUS-Phatas simulation software [14] that solves the structural dynamics of a wind turbine, thus enabling full aeroelastic interaction.

In the current set-up, several engineering extensions are used by the BEM model identical to previously reported set-ups [9]. The airfoil data used both for the BEM and AWSM code originate from dedicated 2D tests [15] with modifications in the form of a 3D rotational correction and dynamic stall model of Snel [16,17]. The AWSM code computational setup has been based on previous convergence studies and the wake length has been extended to approximately three rotor diameters downstream of the rotor. Unless otherwise indicated the time step of the simulations is set to equal 10° rotor azimuth. The applied wake reduction technique in AWSM consisted of one transition zone from where the shed vorticity lines were coarsened, usually applied after one rotation. Differently, for the shed skipping technique several transition zones were prescribed. The AWSM code was ran on a computer that allowed parallelization over 40 cores.

The **CNR-INSEAN FUNAERO** solver features a potential flow aerodynamic formulation for incompressible, inviscid and irrotational flows around 3D lifting bodies in unsteady motion [4, 18]. The integral solution of the Laplace equation governing the flow field is derived by applying the unbounded-space Green function technique [19] to obtain a superposition of singularities on the actual surface of the rotor blades (sources and vortices) and their wakes (vortices). The velocity potential upon the blades is evaluated through discretization of blades and wakes surfaces and application of a *zero-th* order Boundary Integral Equation Method (BIEM). Blade loads are finally calculated by integration of blade pressure distribution provided by the Bernoulli equation. A flow-aligned unsteady free-wake solution scheme is adopted to characterize the behavior of trailing and shed vortices. A thorough analysis of the numerical convergence of the algorithm along with guidelines for the choice of the corresponding numerical parameters setup is provided in [20]. The FUNAERO solver is suitable to efficiently predict rotor airloads and wake inflow under attached flow operating conditions whilst viscosity effects (like, for instance, unsteady flow separation occurring in off-design operations) can be approximately described through inclusion of suitable models. To this aim, FUNAERO has been combined to the Beddoes–Leishman airfoil theory for dynamic stall [21], the Viterna–Corrigan approach [22] for deep stall regimes and the empirical corrections based on the laminar boundary layer theory [16] for centrifugal effects. FUNAERO is also coupled to an aeroelastic formulation based on the Finite Element Method (FEM) for performance and stability predictions [23]. The wake reduction technique implemented in FUNAERO consists in a variable number of transitions with the option of defining an analytical function to achieve a continuous coarsening of wake grid in streamwise direction. For the aim of the present work, a rough estimation of the viscosity-induced tangential stresses is achieved under the simplified assumption that the boundary layer on the blade surface behaves like that over a flat plate at Reynolds number matching turbine operating conditions. The time step of the simulations is always set to equal 6° rotor azimuth. The FUNAERO code was ran on a cluster that allowed parallelization over 36 cores in a shared memory environment.

3.2. Load cases

For uniform axial inflow conditions, a traverse through the operational regime is performed from very low thrust values (featuring a high local angle of attack and separated flow), to design conditions and to high loading in the turbulent wake state. Several representative unsteady load cases were also selected: three cases in 30° yawed flow, a hypothetical case featuring large vertical wind shear (power law exponent $\alpha = 1$) and a dynamic inflow case featuring two fast pitch steps. Finally, a normal production load case in partial load is subject of investigation, featuring a rigid version of the 200 m AVATAR 10MW rotor in turbulent inflow. Here time varying pitch and rotational speed have been prescribed as obtained from a BEM simulation with controller to ensure realistic local inflow conditions. An overview of the cases is given in Table 1.

Table 1. Load case overview.

Name	Nr. cases [-]	Rotor$^{\pm}$	U_∞ [m/s]	Pitch angle [°]	Rot. speed [rpm]	TSR [-]	BEM	AWSM	FUN-AERO†
Axial flow	9	M	7-30	-2.3	425	3-13	x	x	x
Yawed flow (30°)	3	M	10-24	-2.3	425	4-10	x	x	
Sheared flow	1	M	14.9$^{\mp}$	-2.3	425	6.7	x	x	x
Dynamic inflow	1	M	10.0	steps	425	10.0	x	x	
Turbulent inflow	1	A	8.0‡	0.0	var*	var*	x	x	

$^{\pm}$ M = Mexico, A = AVATAR † Attached flow cases only $^{\mp}$ Power law exp. $\alpha = 1$
‡ Time averaged hub height wind speed, class A NTM stochastic field
* Prescribed temporal variation based on BEM simulation with controller

4. Results

4.1. Axial flow

Since computational time and its saving mainly depend on the used number of wake points, they can be regarded irrespective of the load case under consideration. For axial flow, a full tip speed ratio (λ) traverse was simulated both by the panel and lifting line codes. The design load case was taken to study the effect on the computational effort of the proposed wake models. A summary of the results is given in Table 2. For the shed skipping approach in AWSM, almost 30% of CPU-time saving can be achieved at a small expense in the prediction of axial force (F_{ax}) and power (P). However, progressively coarsening the wake geometry resolution after one wake revolution for the wake reduction technique, results in up to 79% CPU-time reduction at a comparable expense in accuracy. Based on these results it was decided to focus on the wake reduction technique rather than the shed skipping approach. The FUNAERO results are even more promising for the wake reduction technique in terms of CPU saving and accuracy, which is attributed to the usage of multiple transition zones. The same wake reduction configurations as reported have been used for all the load cases herein considered.

A visualization of the impact of this technique on the load prediction is given in Figure 2. The effect of the wake reduction technique is indicated by the lighter colored band for the configurations outlined in Table 2, where the reference is indicated by the darker colored line. BEM results are shown as well to identify the added value of the vortex wake methods. For the low thrust cases up to the design load case (λ=6.7), the effect of reducing the far wake grid resolution is small judging by the axial force coefficient predicted by AWSM in Figure

Table 2. Result of wake coarsening techniques for New Mexico design load case (U_∞=14.93 m/s, λ=6.7, pitch=-2.3°).

Code	Applied technique†	Revolutions before transition [revs]	Skip shed vortices [-]	Tot. shed vortices [-]	ΔCPU* [%]	ΔP* [%]	ΔF_{ax}* [%]
AWSM	0	-	0	541	-	-	-
AWSM	1	1	1	288	-58	0.8	0.3
AWSM	1	1	2	204	-71	1.8	0.7
AWSM	1	1	3	162	-79	2.9	1.1
AWSM	2	2/4	1/3	198	-27	2.0	0.8
BEM	-	-	-	-	-99	-3.4	-2.3
FUNAERO	0	-	0	481	-	-	-
FUNAERO	1	2/4‡	2/3	261	-81	0.3	0.1
FUNAERO	1	1/4	2/3	231	-78	0.8	0.4
FUNAERO	1	2/4	3/4	221	-87	0.0	0.0
FUNAERO	1	1/4	3/4	181	-92	0.8	0.4

† 0=reference, 1=wake reduction, 2=shed skipping * Δ with respect to reference (0)
‡ Two transitions are used in FUNAERO

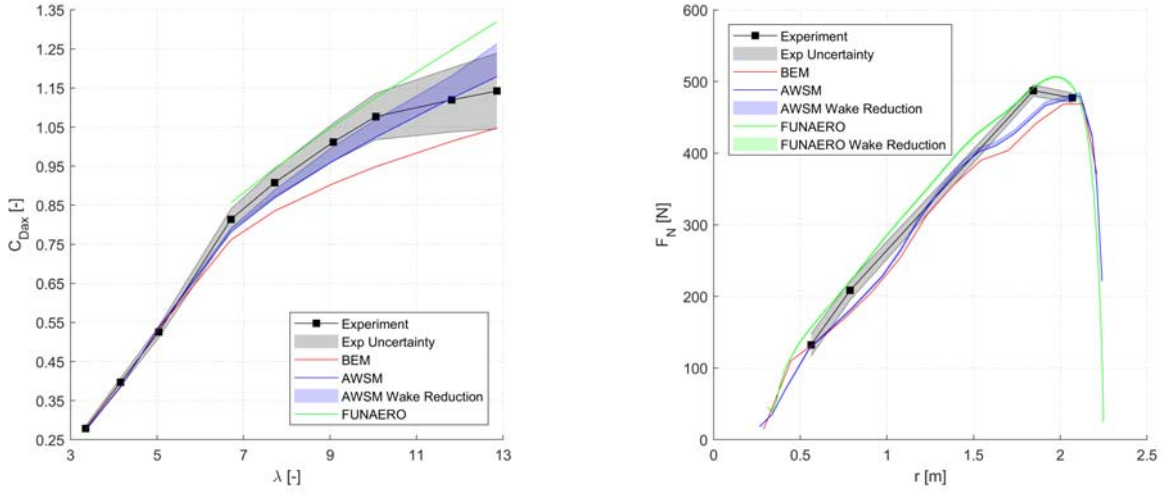

(a) Rotor axial force coefficient as a function of λ.

(b) Blade distribution of chord normal force (λ=6.7).

Figure 2. Effect of wake reduction on loading in axial inflow for the Mexico rotor.

2(a). Above this condition this effect progressively increases the predicted loading. A look into the wake geometry (not shown here) reveals the transition zone to be relatively close to the rotor due to the high rotor induction. Hence, rather than specifying the start of the transition zone in terms of rotor revolutions, it is better to define it in terms of downstream distance (approximately half a diameter when using a 10° azimuth time step). Moreover, it is shown that including multiple transition zones reduces the sensitivity of predicted loads to wake reduction. The agreement between experiment and simulations is very good up to design load conditions.

Inspecting the spanwise distribution of normal force in design load conditions (Figure 2(b)) also reveals a generally good agreement. However axial force results seem to slightly diverge for high tip speed ratios towards the turbulent wake state. It is hypothesized that BEM starts to suffer from not accounting for radial expansion effects and the lack of physics included in the turbulent wake state model. The difference between the two vortex wake models is attributed to the usage of airfoil data, which seems to differ from the panel method calculated pressure distributions. However the approximation of viscous effects in the latter can also add to the uncertainty. It is also noted that these conditions feature relatively low tunnel speeds and consequently low dynamic pressures utilizing only a small fraction of the measurement range (plus the fact that absolute differences are non-dimensionalized with a lower velocity enlarging differences in C_{Dax}). A more detailed comparison between experiment and simulations is illustrated in [24].

4.2. Yawed and sheared inflow

The results of the design load cases in *yaw* are illustrated in Figure 3. The wake reduction approach results in a small increase of the steady blade chord normal force component, similar to the axial inflow case. The load variation (trend) is hardly influenced as depicted by the first 4 blade passage frequencies (i-P) magnitude shown in Figure 3(b). The other two load cases in yaw (not shown here) reveal a similar behavior. It can also be observed that the AWSM trend is very much in line with the experiment, where BEM clearly falls short. The level offset between experiment and simulations is in line with the axial flow case at 82%R and is attributed to the difference between the used airfoil data and real sectional performance. Similar conclusions can be drawn for the other blade forces and moments and at different blade sections.

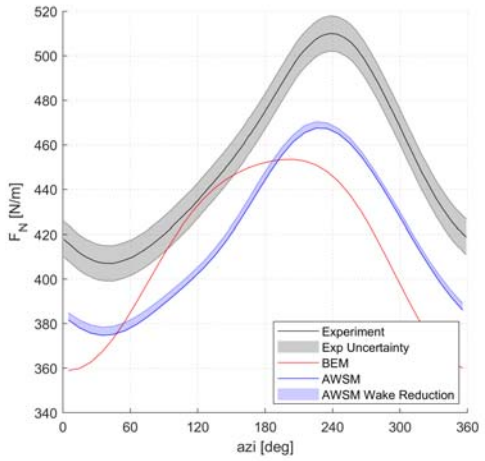

(a) Blade chord normal force variation at 82%R.

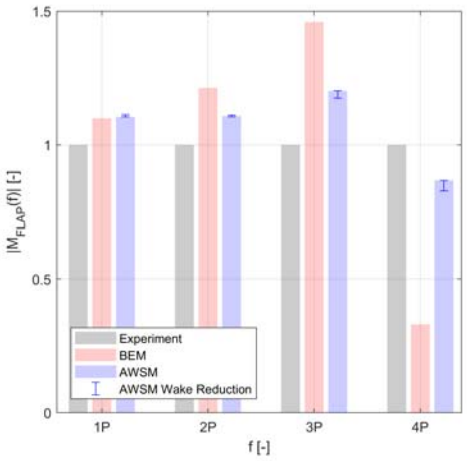

(b) 1, 2, 3 and 4P magnitudes of the flapwise blade root moment, referenced by experimental value.

Figure 3. Effect of wake reduction for yawed flow (30°), Mexico rotor, λ=6.7.

Although no experimental data is available for the *shear* case, the comparison to the FUNAERO code is provided. From Figure 4(a) there is a small positive offset in loading due to the application of wake reduction for the AWSM code, in line with the previous load cases. The FUNAERO result shows a small load decrease when the blade is in the downward position (180° azimuth). The harmonics analysis in Figure 4(b) indicates a small effect on the dynamic loading characteristics, most noticeable for the higher harmonics. The offset between AWSM and FUNAERO are in line with the previous comparisons for the high magnitude harmonics (1 and

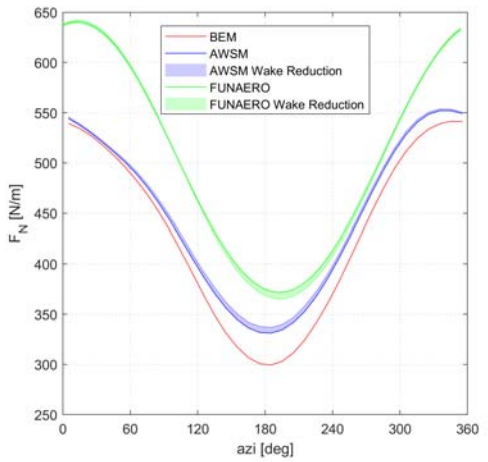

(a) Blade chord normal force variation at 82%R.

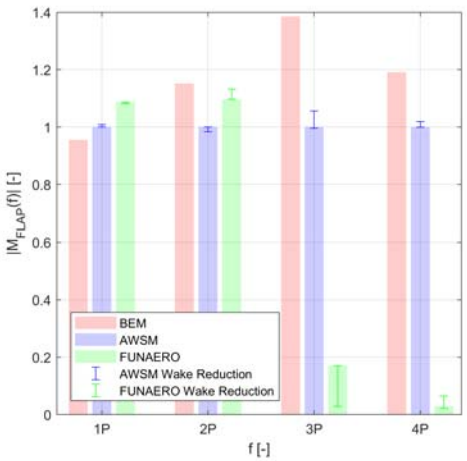

(b) 1, 2, 3 and 4P magnitudes of the flapwise blade root moment, referenced by AWSM value.

Figure 4. Effect of wake reduction for extreme sheared inflow ($\alpha = 1$), Mexico rotor, λ=6.7.

2P), whilst increasing discrepancies arise at 3 and 4P where unsteady flow separation phenomena (not modelled in the panel code) can affect those harmonics magnitudes that, however, are very small in terms of absolute value. Also, Figure 4 clearly shows that BEM overestimates the load fluctuation in comparison to AWSM, which is due to the fact that induction variations in BEM are smoothed out over the annular streamtube. Although this difference may seem small it can be regarded as a canonical case for turbulent inflow conditions, imagining a blade slicing through turbulent eddies, which dominates blade fatigue loading.

4.3. Dynamic inflow

Coarsening the wake resolution is expected to have an impact on dynamic loading in case of sudden wake geometry changes. A *dynamic inflow* case featuring two pitch steps, first from -2.3° to 5° and then back to -2.3° again, is illustrated here. For this case the Mexico turbine is operating at a relatively high thrust (λ=10) and the time step is set to approximately 6° azimuth. Figure 5 indicates that, apart from the small level offset, both the initial load overshoot as well as the damping caused by the wake inertia are preserved. The latter effect is seen to be modeled superiorly by AWSM in comparison to the poor agreement with the experiment for BEM, which returns to the equilibrium value too soon.

4.4. Turbulent inflow

A rigid version of the AVATAR rotor is used with a *turbulent* windfield as defined in Table 1. The time step is set to approximately 4° azimuth, depending on the prescribed rotor speed variations. Fatigue loads are determined over a 4 minute time series. The tabulated results in Figure 6 indicate that the applied wake reduction configurations hardly influence the fatigue loads, also illustrated by the time trace of normal force at 82%R. This can be explained by the fact that the AVATAR rotor operates at a relatively low thrust coefficient, together with the fact that the time step in terms of azimuth angle is smaller than for the other load cases (i.e. the wake description suffers less from linearization of its curved shape). In agreement with the sheared inflow case, the BEM results feature larger load fluctuations resulting in a 7.4% higher damage equivalent load for the blade root flapwise moment.

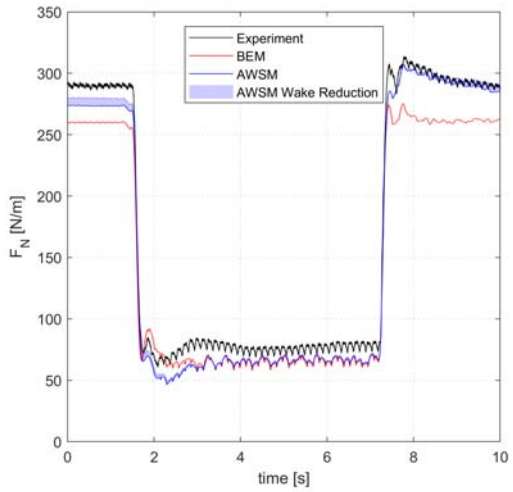

(a) Time trace of blade chord normal force at 82%R.

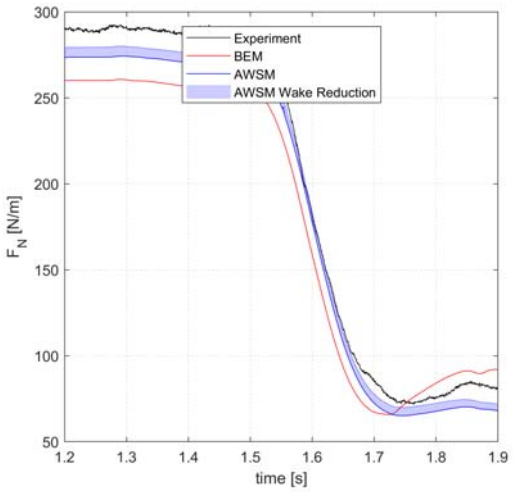

(b) F_N time trace during pitch step from -2.3° to 5°.

Figure 5. Effect of wake reduction for a pitch step (-2.3° → 5° → −2.3°), Mexico rotor, λ=10.

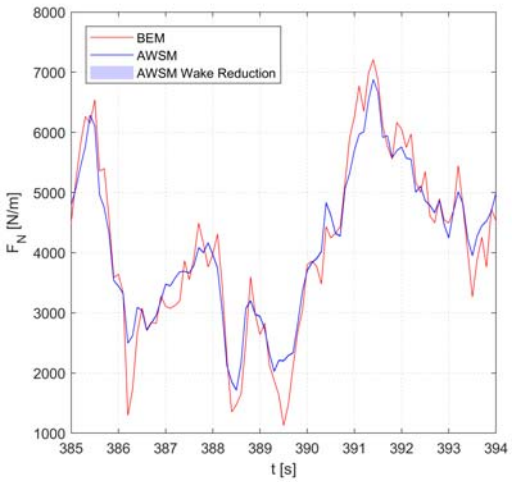

(a) Time trace of chord normal force at 82%R

Configuration		$\Delta M^{\dagger}_{flap,eql}$
Revs before transition [rev]	Skip shed vortices [-]	[%]
1	1	-0.01
1	2	0.08
1	3	0.00
BEM		7.40

† Difference with respect to AWSM reference case

Figure 6. Effect of wake reduction for turbulent inflow load case, AVATAR rotor.

5. Conclusions

A cost-effective free-wake model has been investigated that requires limited programming effort to existing codes and can be considered as an engineering method making approximations to free vortex wake theory. The resolution of the far wake is reduced by progressively skipping shed vortices. The effect of this approach on loading characteristics has been investigated for a variety of load cases, from steady axial inflow to yawed flow, a dynamic pitch step and a turbulent inflow case. Results indicate that generally speaking dynamic and time averaged loading characteristics are preserved when the mid to far wake grid resolution is reduced, whilst CPU-time reductions of 60% to 90% are obtained. An offset in the average load levels can be found if the grid coarsening is initialized too close to the rotor plane. Gradually coarsening the wake grid resolution by using multiple transition zones is more efficient. In the end the preferred

wake reduction configuration depends on the application and the accuracy needed. Concluding it can be stated that the applied wake engineering model is a promising technique bringing us desktop design load calculations using vortex wake methods.

Acknowledgments
The present work has been supported by the Project FARWING funded by the EU IRPWind Mobility Programme, the EU AVATAR project and TKI Wind Op Zee.

References

[1] J.G. Schepers et al. Latest results from the EU project AVATAR: Aerodynamic modelling of 10 MW wind turbines. *J. Phys. Conf. Ser.*, 753(2):022017, 2016.
[2] N. N. Sørensen et al. Engineering models for complex inflow situations. Technical Report AVATAR Deliverable 2.8, 2017.
[3] H.D. Currin et al. Dynamic Prescribed Vortex Wake Model for AERODYN/FAST. *J. Sol. Energ.*, 120, August 2008.
[4] L. Greco, R. Muscari, C. Testa, and A. Di Mascio. Marine Propellers Performance and Flow-Field Features Prediction by a Free-Wake Panel Method. *J. Hydrodyn., Ser. B (English Ed.)*, 26(5):780–795, 2014.
[5] A. van Garrel. *Multilevel panel method for wind turbine rotor flow simulations.* PhD thesis, Univ. of Twente, 2016.
[6] M. Belessis, P. Chasapogiannis, and S. Voutsinas. Free-wake modelling of rotor aerodynamics: recent developments and future perspectives. In *EWEC 2001*, July 2001.
[7] Y.-X. Qiu, X.-D. Wang, S Kang, M. Zhao, and J.-Y. Liang. Predictions of unsteady HAWT aerodynamics in yawing and pitching using the free vortex method. *Renew. Energ.*, 70:93–106, 2014.
[8] D. Marten, M. Lennie, G. Pechlivanoglou, C. Nayeri, and C. Paschereit. Implementation, optimization, and validation of a nonlinear lifting line-free vortex wake module within the wind turbine simulation code Qblade. *ASME J. Eng. Gas Turbines Power*, 138(7):072601–1–072601–10, 2015.
[9] K. Boorsma, M. Hartvelt, and L.M. Orsi. Application of the lifting line vortex wake method to dynamic load case simulations. *J. Phys. Conf. Ser.*, 753(2):022030, 2016.
[10] K. Boorsma and J.G. Schepers. Rotor experiments in controlled conditions continued: New Mexico. *J. Phys. Conf. Ser.*, 753(2):022004, 2016.
[11] K. Boorsma, F. Grasso, and J.G. Holierhoek. Enhanced approach for simulation of rotor aerodynamic loads. Technical Report ECN-M–12-003, ECN, EWEA Offshore 2011, Amsterdam, Nov.-Dec. 2011, 2011.
[12] C. Lindenburg and J.G. Schepers. Phatas-IV aeroelastic modelling, release "dec-1999" and "nov-2000". Technical Report ECN-CX–00-027, ECN, 2000.
[13] A. Van Garrel. Development of a wind turbine aerodynamics simulation module. Technical Report ECN-C–03-079, ECN, 2003.
[14] http://www.wmc.eu/focus6.php. 2016.
[15] K. Boorsma and J.G. Schepers. New mexico experiment, description of experimental setup. Technical Report ECN-X-15-093 (v3), ECN, 2018.
[16] H. Snel, R. Houwink, J. Bosschers, W.J. Piers, G.J.W. van Bussel, and A. Bruining. Sectional prediction of 3-D effects for stalled flow on rotating blades and comparison with measurements. In *Proc. of the European Community Wind Energy Conference*, 1993.
[17] H. Snel. Heuristic modelling of dynamic stall characteristics. In *Proc. European Wind Energy Conference*, pages 429–433, Dublin, Ireland, October 1997.
[18] A. Calabretta, M. Molica Colella, L. Greco, and M. Gennaretti. Assessment of a comprehensive aeroelastic tool for horizontal-axis wind turbine rotor analysis. *Wind Energy*, 19(12):2301–2319, December 2016.
[19] L. Morino. Boundary integral equations in aerodynamics. *Appl. Mech. Rev.*, 46(8):445–466, 1993.
[20] L. Greco, F. Salvatore, and F. Di Felice. Validation of a quasi-potential flow model for the analysis of marine propellers wake. In 25^{th} *ONR Symposium on Naval Hydrodynamics (ONR 2004)*, August 2004.
[21] J.G. Leishman and G.L.Jr. Crouse. State-Space Model for Unsteady Airfoil Behavior and Dynamic Stall, AIAA Paper 1989. In 30^{th} *Structures, Structural Dynamics and Materials Conference*, 1989.
[22] J. Martinez, L. Bernabini, O. Probst, and C. Rodriguez. An improved BEM model for the power curve prediction of stall-regulated wind turbines. *Wind Energy*, 8(4):385–402, 2005.
[23] A. Calabretta, C. Testa, L. Greco, and M. Gennaretti. Assessment of a a FEM-based Formulation for Horizontal Axis Wind Turbine Rotors Aeroelasticity. *Appl. Mech. Mater.*, 798:75–84, October 2015.
[24] K. Boorsma and J.G. Schepers et al. Final report of IEA Task 29: Mexnext (Phase 3). ECN-E-18-003, Energy Research Center of the Netherlands, 2018.